Biomedicine & Pharmacotherapy 161 (2023) 114548

Contents lists available at ScienceDirect

Biomedicine & Pharmacotherapy

journal homepage: www.elsevier.com/locate/biopha

Trabectedin modulates macrophage polarization in the tumor-microenvironment. Role of $K_V1.3$ and $K_V1.5$ channels

Diego A. Peraza [a,*], Adrián Povo-Retana [a], Marina Mojena [a], Ana B. García-Redondo [b,c,d], Pablo Avilés [e], Lisardo Boscá [a,d], Carmen Valenzuela [a,d,*]

[a] Instituto de Investigaciones Biomédicas Alberto Sols (CSIC-UAM), 28029 Madrid, Spain
[b] Department of Physiology, Faculty of Medicine, Universidad Autónoma de Madrid, 28029 Madrid, Spain
[c] Hospital La Paz Institute for Health Research (IdiPAZ), 28046 Madrid, Spain
[d] Centro de Investigación Biomédica en Red Enfermedades Cardiovasculares (CIBERCV), 28029 Madrid, Spain
[e] Departamento de Toxicología y Farmacología Preclínica, PharmaMar S.A., 28770 Colmenar Viejo, Madrid, Spain

ARTICLE INFO

Keywords:
Macrophages
Trabectedin
Cancer
TAMs
$K_V1.3$
$K_V1.5$

ABSTRACT

Immune cells have an important role in the tumor-microenvironment. Macrophages may tune the immune response toward inflammatory or tolerance pathways. Tumor-associated macrophages (TAM) have a string of immunosuppressive functions and they are considered a therapeutic target in cancer. This study aimed to analyze the effects of trabectedin, an antitumor agent, on the tumor-microenvironment through the characterization of the electrophysiological and molecular phenotype of macrophages. Experiments were performed using the whole-cell configuration of the patch-clamp technique in resident peritoneal mouse macrophages. Trabectedin does not directly interact with $K_V1.5$ and $K_V1.3$ channels, but their treatment (16 h) with sub-cytotoxic concentrations of trabectedin increased their K_V current due to an upregulation of $K_V1.3$ channels. In vitro generated TAM (TAM_{iv}) exhibited an M2-like phenotype. TAM_{iv} generated a small K_V current and express high levels of M2 markers. K^+ current from TAMs isolated from tumors generated in mice is a mixture of K_V and K_{Ca}, and in TAM isolated from tumors generated in trabectedin-treated mice, the current is mostly driven by K_{Ca}. We conclude that the antitumor capacity of trabectedin is not only due to its effects on tumor cells, but also to the modulation of the tumor microenvironment, due, at least in part, to the modulation of the expression of different macrophage ion channels.

1. Introduction

Ion channels present in the plasma membrane of macrophages make up a perfectly orchestrated network that regulates the resting membrane potential (E_m), contributing to the signaling of intracellular Ca^{2+} and therefore, to their regulation of gene expression [1–9]. Macrophage ion channels pattern vary depending on their state of polarization [3,6,7]. Several potassium currents have been described in macrophages, the K_V current generated by the activation of $K_V1.3/K_V1.5$ heterotetrameric channels [10,11]; the inward rectification potassium current generated by $K_{ir}2.1$ channels (I_{K1}) [12] and the K^+ activated by Ca^{2+} generated by $K_{Ca}3.1$ channels [13,14]. In addition, entry of Ca^{2+} into macrophages through CRAC channels, which are formed by the transmembrane pore-forming subunit ORAI1 in the plasma membrane and a Ca^{2+} sensor STIM1 present in the plasma of the endoplasmic reticulum (ER) [15]. Different stimuli may change the stoichiometry of these heterotetrameric K_V channels. Thus, proliferation and classical activation (M1) of macrophages increase the K_V current by: a) increasing the $K_V1.3/K_V1.5$ ratio, and/or b) forming a certain degree of $K_V1.3$ homotetramers. However, alternative activation decreases the heterotetrameric channel ratio [3,6].

Macrophages play a crucial role in the inflammatory response, acting as antigen-presenting cells and as cells to modify the production of cytokines in the environment and, therefore, the intensity of the response of T lymphocytes [16–19]. In cancer, tumor-associated macrophages (TAMs) exhibit an immunosuppressive phenotype in which they lose their anti-tumor capacity [20–23]. This protumoral capability makes them useful therapeutic targets to prevent tumor growth [24–26]. Modulating the polarization of TAMs towards a pro-inflammatory/anti-tumor phenotype (reeducation) would be

* Correspondence to: Instituto de Investigaciones Biomédicas Alberto Sols (CSIC-UAM), Arturo Duperier 4, 28029 Madrid, Spain.
E-mail addresses: daperaza@iib.uam.es (D.A. Peraza), cvalenzuela@iib.uam.es (C. Valenzuela).

https://doi.org/10.1016/j.biopha.2023.114548
Received 5 December 2022; Received in revised form 3 March 2023; Accepted 14 March 2023
Available online 20 March 2023

therapeutically useful [27–34].

Trabectedin is an anti-tumor drug that blocks the oncogenic transcription, interfering with the cell cycle of tumor cells and causing their apoptosis, but it also affects the tumor microenvironment [25,35–38]. In this study, we analyzed the effects of trabectedin on macrophage I_{K1} and K_V currents. We observed that trabectedin does not produce direct effects on the $K_V1.3$ or $K_V1.5$ channels. However, after 16 h of incubation with the drug, a decrease of the I_{K1} and an increase in the K_V current were observed, both in peritoneal macrophages and TAM_{iv}, due to an increase in the expression of $K_V1.3$. We conclude that the anti-tumor capacity of trabectedin is not only due to its effects on tumor cells and its ability to produce selective depletion of monocytes and macrophages, but also to the modulation of the tumor microenvironment, due, at least in part, to the modulation of the polarization of the macrophages present in the tumor.

2. Materials and methods

2.1. Animal experimentation

Animals were cared for according to the protocol approved by the Ethical Committee of our institution (following directive 2010/63/EU of the European Parliament and Recommendation 2007/526/EC regarding the care of experimental animals, enforced in Spanish law under Real Decreto 53/2013, and approved by the Institutional Ethics Committee (PROEX 197/18). C57BL/6 J male mice were housed under controlled conditions at 25 °C in 12-hour light/dark cycles with ad libitum access to water and food in an environment with maintained temperature and relative humidity.

2.2. Peritoneal macrophages

The mice were killed with CO_2 and resident peritoneal macrophages were obtained and cultured from C57BL/6 J male mice, aged 3–4 months as described [39,40]. Cells were cultured overnight (16 h) without polarization (resting) or polarized (M1 or M2) with their respective stimuli (LPS 100 ng/ml or IL-4 + IL-13 20 ng/ml, each). Trabectedin was added to the culture medium 16 h before each experiment. In some cases, to increase the number of peritoneal macrophages, animals were inoculated with BD Difco™ thioglycollate medium (Thermo Fisher Scientific).

2.3. Tumor-associated macrophages in vitro

In vitro generated tumor-associated macrophages (TAM_{iv}) were obtained by co-culturing resting peritoneal macrophages with a mouse ovarian cancer tumor cell line (ID8) (American Type Culture Collection (ATCC)). Co-culture was performed in transwell cell culture plates (Corning) and maintained at 37 °C in a 5% CO_2 atmosphere. Peritoneal macrophages were seeded in the lower part of the transwell and ID8 cells in the permeable support and cultured in supplemented DMEM for 48 h. The pore diameter (0.4 μm) only allows the passage of soluble metabolites synthesized by the cells. Trabectedin was added to the co-culture medium 16 h before using TAM_{iv}.

2.4. Tumor-associated macrophages

Tumor-associated macrophages (TAM) from tumor-bearing mice treated with trabectedin 0.15 mg/Kg or with vehicle were obtained as described next. Cell derived xenografts from human gastric carcinoma line HGC27 was grafted subcutaneously to the flank of 4- to 6-week-old nu/nu athymic mice near the hind paw. The grafts took about 10 days to reach a size of 300–400 mm^3, at which point they were randomly distributed between the control and treated groups. Those in the control group received an intravenous injection of vehicle (aqueous solution containing sucrose, potassium dihydrogen phosphate and pH correctors - phosphoric acid and potassium hydroxide) and those in the treatment group received a single intravenous injection of trabectedin 0.15 mg/kg. Mice were sacrificed 24 h after injection and tumors were obtained for analysis. In no case did the tumors exceed 500 mm^3 in size. Each tumor was cut into small fragments (< 2 mm) in a Petri dish with serum-free RPMI containing collagenase (0.5 mg/ml), hyaluronidase (0.1 mg/ml) and DNAase 200 U/ml and this mixture was incubated at 37 °C for 30 min with gentle shaking. Then, the fragments not digested by the enzyme were disaggregated by gentle pipetting and filtered initially at 100 μm and then at 40 μm, washing with 20 ml PBS each time. This solution was centrifuged at 300 g for 5 min at room temperature. The pellet was resuspended in 10 ml of cold MACS buffer (PBS with 0.5% BSA and 2 mM EDTA). The cells were centrifuged again at 300 g for 5 min at 4ºC and the pellet was resuspended in 90 μl MACS buffer per 110 cells and 10 μl of Fc-receptor blocking reagent (Miltenyi Biotec) was added and incubated for 10 min at 4ºC. Then, 10 μl of magnetic beads coated with anti-CD11b (Miltenyi Biotec) were added and incubated for 15 min at 4ºC. Cells were washed with MACS buffer and CD11b positive cells were separated using a magnetic separation system (MidiMACS separator with LS columns, Miltenyi Biotec) according to the manufacturer's instructions. TAMs (CD11b-positive cells) were collected in 5 ml of ice-cold MACS buffer, removed from the LS column of the magnetic support and kept on ice for the minimum time necessary for processing in electrophysiology experiments. Likewise, resident peritoneal macrophages of these tumor-bearing mice were extracted by peritoneal lavage, as described in the previous section. TAMs and peritoneal macrophages of tumor-bearing mice were obtained from PharmaMar S.A. were seeded in plates for cell culture (Falcon) in supplemented DMEM and maintained for 16 h at 37ºC in a 5% CO_2 atmosphere.

2.5. Flow cytometry

Macrophages were seeded at a concentration of 0.5–1 × 10^6 cells/well. 16 h before flow cytometry assays, resting, M1 and M2 macrophages, as well as TAM_{iv}, were treated with increasing concentrations of trabectedin (0–150 nM). Macrophages supernatants were preserved, cells were treated with TrypLETM Express recombinant proteases (Thermo Fisher Scientific) and after 4 min at 37 °C in a 5% CO_2 atmosphere, trypsin was neutralized with sterile PBS with 2% FBS. Cells were collected and centrifuged at 300 g for 5 min at 4 °C. The supernatants were discarded and macrophages were incubated with different probes for 30 min (see the following sections). 4',6 Diamidino-2-phenylindole or DAPI (1:1000) was added to all the cytometer tubes 5 min before measuring the signal on the FACS-Canto II flow cytometer (Becton Dickinson) from the Interdepartmental Research Service (SIdI) from the UAM, using the BD FACSDivaTM program (BD Biosciences). The data was processed using the FlowJo™ v10 program (FlowJo).

To analyze cell viability, cell media preserved were always centrifuged and properly considered for all cell viability determinations. The Annexin V FITC probe (Immunostep) (2 μl/well) was diluted in the Annexin V binding buffer (1 ×) (Immunostep). Therefore, we stained simultaneously with DAPI, to discriminate intact macrophages (Annexin V FITC-, DAPI-), early apoptosis (Annexin V FITC+, DAPI-), late apoptosis (Annexin V FITC+, DAPI+) and macrophages in a state of necrosis (Annexin V FITC-, DAPI+).

To measure reactive oxygen species (ROS) DCFH-DA fluorescent probe was used (2'7'dichlorofluorescin diacetate, Sigma-Aldrich). The probe was prepared according to the manufacturer's instructions. It was dissolved in DMSO and stored at − 20ºC. The probe was used at a concentration of 5 μM, dissolved in PBS with 2% FBS.

MitoTracker® Red CMXRos probe (Invitrogen) allowed us to differentiate macrophages with a compromised mitochondrial membrane potential (Ψ). The CMXRos probe was prepared according to the manufacturer's instructions. It was dissolved in DMSO and stored at − 20ºC, protected from light. The probe was used at a concentration of 100 nM, dissolved in PBS with 2% FBS.

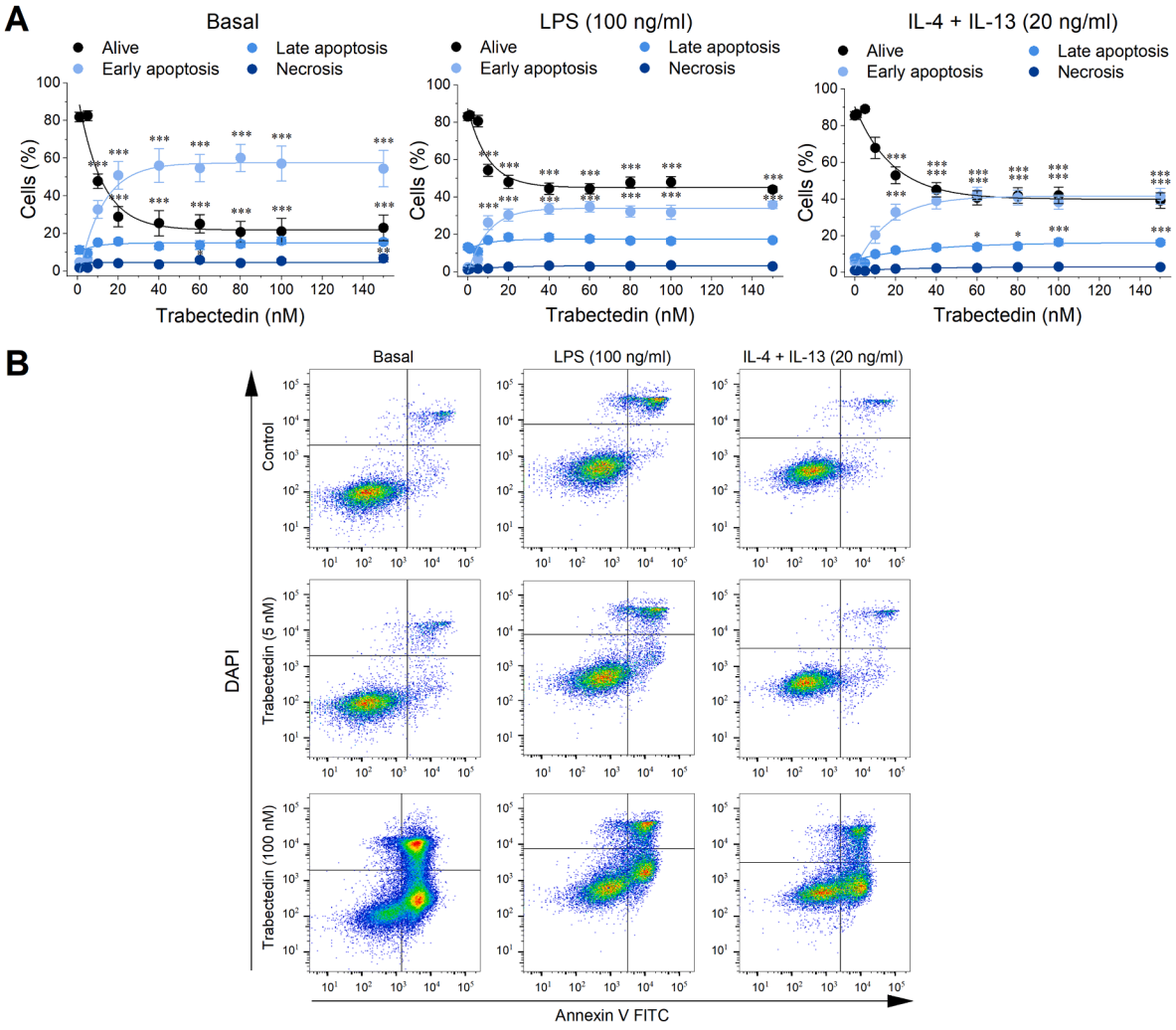

(caption on next page)

Fig. 1. Effects of trabectedin on viability, ROS and mitochondrial membrane potential of peritoneal macrophages. (A) Plot of the percentage of live macrophages, early apoptosis, late apoptosis or necrosis of the different polarization states (resting, LPS 100 ng/ml or after IL-4 & IL-13 20 ng/ml) treated or not with different concentrations of trabectedin (0–150 nM). (B) Dot-plot of Annexin V FITC/DAPI obtained by flow cytometry representative of different polarization states of macrophages untreated (control) or treated with trabectedin 5 and 100 nM. The right quadrants of each dot-plot (Annexin V FITC+/DAPI- and Annexin V FITC+/DAPI+) represent the apoptotic cells of each condition. (C) Plot of the increase in ROS production by macrophages in different polarization states treated or not with trabectedin (0–150 nM). Values normalized to the 0 nM concentration of each condition (untreated, left). Representative histograms of live macrophages in different polarization states untreated or treated with 5 or 100 nM trabectedin and labeled with DCFH-DA (right). (D) Plot of the increase of the ψ of live macrophages in different polarization states treated or not with trabectedin (0–150 nM). The mean ± SEM of 5–7 experiments is plotted (left). Representative histograms of macrophages in different polarization states, untreated or treated with 5 and 100 nM trabectedin labeled with CMXRos (right). Each point represents the mean ± SEM of 6–7 experiments. Statistical analysis: * $p < 0.05$, ** $p < 0.01$, *** $p < 0.001$ vs. Trabectedin (0 nM) (1-way ANOVA, followed by a Test-Tukey).

2.6. RNA extraction and RT-qPCR assays

Total RNA extraction from macrophages was performed at the IIBm Genomics Service (CSIC-UAM) using RNeasy Micro RNA extraction kit (QIAGEN). RNA sample quality check was performed using an Agilent 2100 Bioanalyzer (Agilent) and the quantity check was measured using the NanoDrop® ND 1000 (Thermo Fisher Scientific). Consecutively, the Applied BiosystemsTM High-Capacity cDNA Reverse Transcription Kit (Thermo Fisher Scientific) was used to perform the reverse-transcription of the RNA obtaining a concentration of 2.5 ng/μl of cDNA. The q-PCR was performed at the IIBm Genomics Service (CSIC-UAM) using the Applied Biosystems 7900 HT Fast Real-Time PCR kit (Thermo Fisher Scientific) using 5 ng of cDNA and SYBR Green probes (Thermo Fisher Scientific) according to the manufacturer's instructions. Three replicates for each cDNA sample were tested. Supplemental Table 1 shows the specific sequences of the primers used in the RT-qPCR experiments. The expression level of each of the genes was quantified, using the formula $2^{-\Delta\Delta Ct}$, where GAPDH served as an internal control.

2.7. Immunofluorescence of $K_V1.3$ (extracellular) channels

$K_V1.3$ channels in the plasma membrane of macrophages were successfully immunostained with a polyclonal anti-$K_V1.3$ antibody directed against an extracellular epitope of the human $K_V1.3$ channel (APC-101, Alomone) as described [40]. Preparations were examined using an LSM710 spectral confocal microscope (Zeiss) in the IIBm Optical and Confocal Microscopy Service (SEMOC) and processed using ZEN2009 image acquisition (Zeiss). Fluorescence intensity was quantified using ImageJ software (NIH).

2.8. Electrophysiology

Potassium currents from macrophages were recorded at room temperature (21–24 °C), using the whole-cell patch-clamp technique with an Axopatch 200B amplifier (Molecular Devices) connected to Digidata 1322 A. Micropipettes were pulled from borosilicate glass capillary tubes (Narishige GD-1) on a programmable horizontal puller (Sutter Instrument Co.) and heat-polished with a microforge (Narishige). Micropipette resistance was 2–4 MΩ. Data acquisition and genesis of experimental protocols were performed by the CLAMPEX utility of the PCLAMP 9.0.1 program (Molecular Devices). Currents were filtered at 2 kHz and sampled at 4 kHz (Bessel filter of 4 poles). The internal pipette filling solution with a free Ca^{2+} concentration of 10^{-9} M ($[10^{-9}$ M $Ca^{2+}]_i$) contained (in mM): 80 K-aspartate, 42 KCl, 3 phosphocreatine, 10 KH_2PO_4, 3 MgATP, 5 HEPES-K^+, 5 EGTA-K^+ and it was adjusted to pH = 7.25 with KOH. The intracellular pipette filling solution with a free Ca^{2+} concentration of 10^{-6} M ($[10^{-6}$ M $Ca^{2+}]_i$) contained (in mM): 150 KCl, 10 NaCl,1.13 $MgCl_2$, 1 $CaCl_2$, 10 HEPES-K^+, 1.1 EGTA-K^+ and it was adjusted to pH = 7.20 with KOH. The bath solution contained (in mM): 145 NaCl, 4 KCl, 1.8 $CaCl_2$, 1 $MgCl_2$, 10 HEPES-Na^+ and 10 glucose and it was adjusted to pH = 7.40 with NaOH. The currents were stored in a computer and analyzed with the CLAMPFIT utility of the PCLAMP 9.0.1 program and Origin 2018 (OriginLab Co.). The K_V and K_{Ca} currents were recorded from a potential holding of − 80 mV after applying different pulse protocols every 20 s at 0.02 Hz to complete the recovery process of the current inactivation avoiding an accumulation of inactivation.

2.9. Calcium time-lapse assays

We used the in vivo Cell Observer system (Carl Zeiss) of the IIBm SEMOC, composed of an inverted, light-transmitted and epifluorescence Z1 Observer microscope coupled with a tightly regulated cell incubator chamber (37 °C in a 5% CO_2 atmosphere) connected to a monochrome, high-resolution camera (Cascade 1 K), 10 × Plan-APOCHROMAT camera lens. Additionally, we assembled a suction system with a vacuum pump and a system that allowed us to change solutions at the right time. Macrophages were seeded at a concentration of 1×10^6 cells/well. Before, they were incubated in equal volumes of a Tyrode solution (1.2 mM Ca^{2+}) containing (in mM): 140 NaCl, 5 KCl, 1.2 $CaCl_2$, 0.5 $MgCl_2$ 10 HEPES-Na^+ and 5 glucose (adjusted to pH = 7.40 with Tris-HCl) and Fluo-4 DirectTM probe (Thermo Fisher Scientific) for 40 min at 37 °C in a 5% CO_2 atmosphere. Later, Fluo-4 DirectTM was removed by washes with Tyrode (1.2 mM Ca^{2+}). After placing the culture plate on the stage of the Cell Observer microscope, we removed the Tyrode (1.2 mM Ca^{2+}) and add Tyrode (0 Ca^{2+}) contained (in mM): 140 NaCl, 5 KCl, 1.7 $MgCl_2$, 10 HEPES-Na^+, 0.5 EGTA and 5 glucose (adjusted to pH = 7.4 with Tris-HCl). At this point, we began to measure the basal fluorescence ([Ca^{2+}] basal) for 5 min. Afterward, thapsigargin (200 nM) (Sigma-Aldrich) in Tyrode (0 Ca^{2+}) was added and we measured the fluorescence for 10 min to analyze the Ca^{2+} output from the endoplasmic reticulum (ER). Finally, the Tyrode (0 Ca^{2+}) was changed to Tyrode (1.2 mM Ca^{2+}) and we measured the fluorescence for another 10 min, thus observing the entry of Ca^{2+} into the cytoplasm through the CRAC channels. The absorption and emission spectra were 494 nm and 516 nm, respectively. Data acquisition and the genesis of the experimental protocol were controlled by the Axiovision Rel. 4.8 system (Thermo Fisher Scientific). The calcium time-lapse assays were analyzed by using the AxioVision program (Thermo Fisher Scientific) and the ImageJ program.

2.10. Statistical analysis

In each series of experiments the mean, standard deviation and standard error of the mean (SEM) were calculated. Data were expressed as the mean ± SEM of a given number (n) of experiments. To analyze the significant differences in blocking at different voltages, use dependency of the current in the absence and in the presence of trabectedin, the Student t-paired data comparison test was used. Comparisons between more than two experimental groups were performed using an analysis of variance (ANOVA), and a subsequent Tukey-test as a post hoc analysis to determine the statistical significance between each group. In both cases, significant differences were considered when the P value turned out to be less than 0.05.

3. Results

3.1. Effects of trabectedin on viability, ROS production and Δψ in different functional states of peritoneal macrophage polarization

Peritoneal macrophage viability, ROS production and Δψ were decreased by trabectedin in a concentration-dependent manner. Each

polarization state of macrophages presents a different degree of sensitivity to trabectedin, but all of them share a similar response based on two types of concentrations as macrophage viability is compromised: sub-cytotoxic (1–10 nM) and cytotoxic (20–150 nM) (Fig. 1A-B). A greater degree of early apoptosis induced by trabectedin sub-cytotoxic concentrations was observed in M0 macrophages ($p < 0.001$ vs. M1), followed by M2 and M1. It should be noted that ROS production related to the apoptotic effect of trabectedin (Fig. 1C) at M0 macrophages have

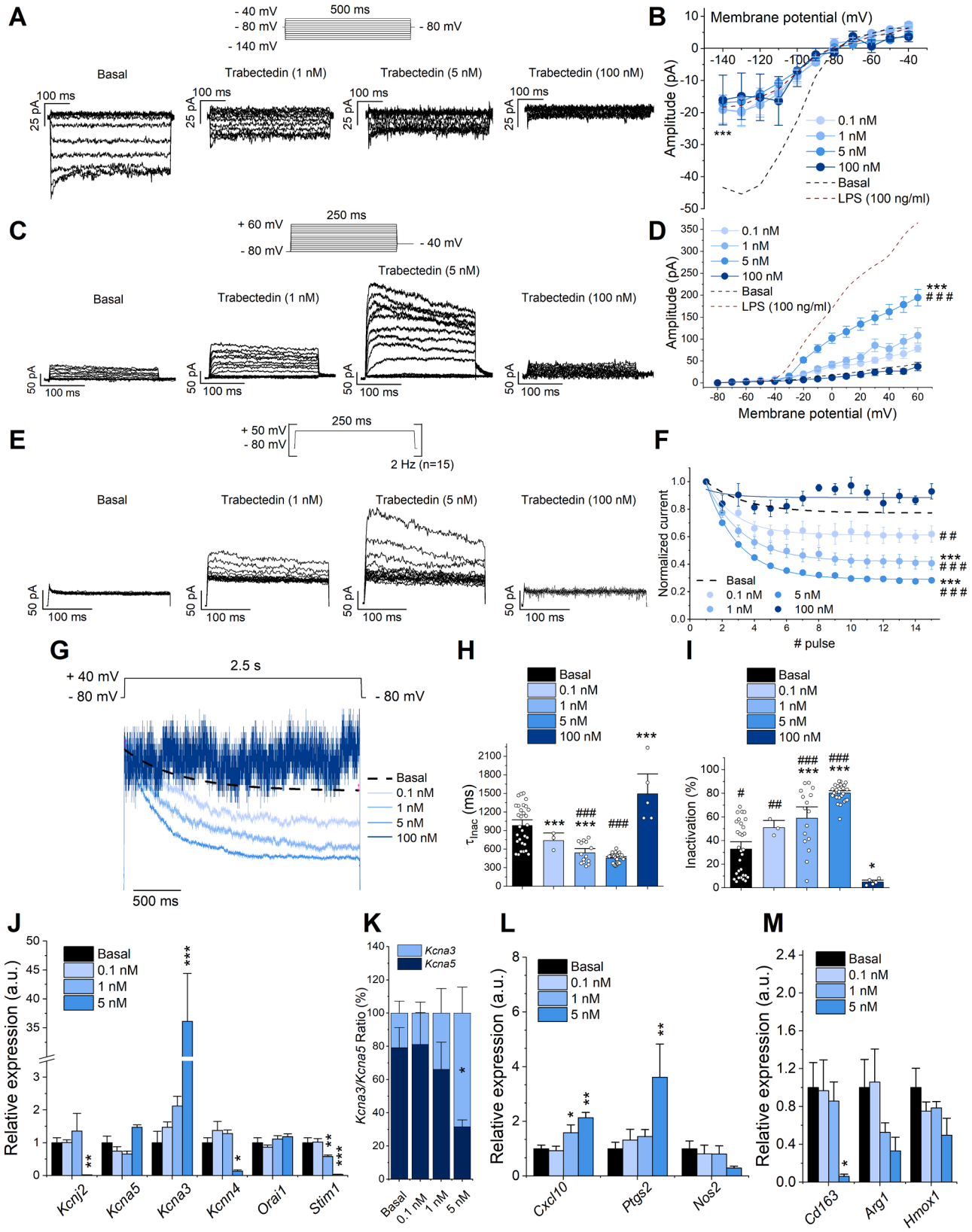

(caption on next page)

Fig. 2. Effects of trabectedin on K_{ir} and K_v currents, on the levels of expression of ion channels and also on M1 and M2 markers of peritoneal macrophages. (A) I_{K1} current traces generated by macrophages treated or not with trabectedin 1, 5 and 100 nM, obtained after applying the pulse protocol shown. (B) I-V ratio of I_{K1} from macrophages treated with 0.1–100 nM trabectedin. Dashed lines show the mean I-V obtained in resting and in LPS (100 ng/ml) conditions. Each point represents the mean ± SEM of 6–26 experiments. (C) Representative recordings of the K_V currents of resting macrophages treated or not with trabectedin (0.1–100 nM), obtained after applying the protocol shown. (D) I-V relationship of K_V currents from macrophages treated or not with trabectedin. Dashed lines show the I-V relationship of the resting and LPS (100 ng/ml) conditions. Each point represents the mean ± SEM of 8–37 experiments. (E) Representative recordings of resting macrophages treated or untreated with trabectedin, obtained after applying the pulse train shown at the top. (F) Use-dependence decay of K_V generated by macrophages treated or not with trabectedin after normalizing the amplitude generated by each pulse against the maximum current of the pulse train versus the number of pulses. Each point represents the mean ± SEM of 5–28 experiments. (G) Representative recordings of resting macrophages treated or not with trabectedin obtained after applying a depolarizing pulse of 2.5 s at + 40 mV. (H) Inactivation kinetics (τ_{Inac}) of the depolarizing pulse of 2.5 s at the different experimental conditions obtained after fitting this process to a monoexponential function. (I) Degree of inactivation during the application of 2.5 s at different experimental conditions shown in panel G. (J) Relative mRNA expression of the genes codifying different ion channels in basal or treated with trabectedin quantified by RT-qPCR. Variation of normalized mRNA versus mRNA present in basal macrophages. The mean ± SEM of 3–9 experiments is plotted. (K) Expression ratio of $K_V1.5$ and $K_V1.3$ measured by RT-qPCR. The mean ± SEM of 4–11 experiments is plotted. (L) Relative mRNA expression of inflammatory genes (*Cxl10*, *Ptgs2* and *Nos2*) from basal or trabectedin-treated macrophages versus mRNA expressed in basal macrophages. The mean ± SEM of 3–9 experiments is plotted. (M) Relative mRNA expression of anti-inflammatory genes (*CD163*, *Arg1* and *Hmox1*) from basal or trabectedin-treated macrophages versus mRNA expressed in basal macrophages. The mean ± SEM of 4–9 experiments is plotted. * $p < 0.05$, ** $p < 0.01$, * ** $p < 0.001$ vs. Resting; # $p < 0.05$, ## $p < 0.01$, ### $p < 0.001$ vs. Trabectedin (100 nM) (1-way ANOVA, followed by a Test-Tukey).

slower exponential kinetics than that of LPS-stimulated macrophages. In contrast, when these cells are polarized to an immunosuppressive phenotype with IL4 +IL13 (M2-like), they turn out to be more resistant. In fact, at the maximum concentration tested, the ROS release produced by M2 macrophages is less than in M0 ($p < 0.05$, $n = 5$) or in M1 macrophages ($p < 0.05$, $n = 6$). We also studied the mitochondrial membrane potential ($\Delta\psi$) to know if the apoptotic effect of trabectedin entails a dysfunction of mitochondrial respiration (Fig. 1D). Trabectedin induced hyperpolarization of the $\Delta\psi$ in a concentration-dependent manner in all three experimental approaches. Thus, the M1 stimulus (LPS) is the only experimental condition in which sub-cytotoxic concentrations seem to hyperpolarize the $\Delta\psi$. In basal or M2 macrophages (IL4 +IL13), the level of hyperpolarization turned out to be similar. Considering all these results, we set out to study whether the functional state of macrophages could be modulated using sub-cytotoxic concentrations of trabectedin that did not compromise the viability of macrophages.

3.2. Effects of trabectedin on potassium ion currents of resting peritoneal macrophages

Supplementary Fig.1 A-H shows the K_{ir} and K_V currents obtained in resting, M1 and M2 macrophages, which resulted be similar to those previously described in other types of macrophages [3,6,8,39]. We then analyzed the effects of trabectedin (100 nM) in the K_V currents generated by M0 macrophages (mostly generated by $K_V1.5$ channels) and LPS-stimulated macrophages (mostly due to the activation of $K_V1.3$ channels) perfused (15 min) with trabectedin (100 nM) (Supplementary Fig. 2A-C). Under these experimental conditions, K_V currents were not modified, suggesting that trabectedin does not produce direct effects on $K_V1.5$ or $K_V1.3$ channels. Thus, we analyzed the electrophysiological characteristics of the K_V currents generated by M0 macrophages after incubation for 16 h with sub-cytotoxic (0.1–5 nM) trabectedin concentrations.

After applying the pulse protocol shown in the upper part of Fig. 2A, K_{ir} currents were recorded. The incubation of resting macrophages with trabectedin (5 nM) decreased the K_{ir} currents ($n = 26$, $p < 0.001$) (Fig. 2A-B). On the contrary, trabectedin increased the magnitude of the K_V current on resting macrophages in a qualitatively similar way to LPS ($n = 38$, $p < 0.001$) (Fig. 2C-D). As shown in Fig. 2E, the trabectedin-induced increase in the amplitude of the K_V current was accompanied by an increase in the use dependency of the current, and by an increase in the degree of inactivation in a concentration-dependent manner. Thus, macrophages incubated with the highest sub-cytotoxic concentration of trabectedin (5 nM) generated a current with a greater percentage of use-dependent decay ($n = 24–28$, $p < 0.001$) (Fig. 2E-F). This degree of use-dependent decay induced by trabectedin (5 nM), is similar to that observed in M1 macrophages ($n = 25–28$, $p > 0.05$). Also, after applying a depolarizing pulse of 2.5 s (Fig. 2G), trabectedin (1 and 5 nM) accelerates the inactivation kinetics of the K_V current ($n = 29–30$, $p < 0.001$) (Fig. 2H) and increased the degree of inactivation ($n = 27–30$, $p < 0.001$) (Fig. 2I).

The electrophysiological changes of K_{ir} and K_V current generated by resting macrophages incubated with trabectedin for 16 h may be indicative of modifications in the expression and composition of the K^+ ion channels present in the macrophages. In fact, Fig. 2J shows changes in the relative expression of RNA of several ion channels present in macrophages. Trabectedin (5 nM) decreased the relative expression of *Kcnj2* and increased the expression of *Kcna3*, which can explain the decrease in K_{ir} and the increase of K_V currents observed in macrophages incubated with trabectedin (5 nM), respectively (Fig. 2J). All these results suggest that trabectedin modifies the $K_V1.3/K_V1.5$ ratio of the heterotetramers that generate K_V currents in macrophages (Fig. 2K). We also analyzed the levels of expression of $K_V1.3$ channel protein at the plasma membrane (Supplementary Fig. 3A-B) by immunofluorescence, observing an increase in $K_V1.3$, suggesting that the increase in the amplitude of the K_V current produced by trabectedin (5 nM) is due to an increase for $K_V1.3$ channel in the macrophage plasma membrane. Therefore, we studied the relative expression of mRNAs of different M1 and M2 markers and we observed that trabectedin increased in expression levels of the pro-inflammatory markers: *Cxcl10 and Ptgs2* (Fig. 2L); and reduced ($p < 0.05$) the expression of the anti-inflammatory marker *Cd163* (Fig. 2M).

3.3. Effects of trabectedin on Ca^{2+} movements of resting macrophages

Due to the crucial role of K_V channels in maintaining the E_m and, thus, in the regulation of $[Ca^{2+}]_i$, we analyzed the effects of trabectedin-incubation on Ca^{2+} movements in M0 macrophages. To that end, we applied the protocol shown in Fig. 3A. First, we observed that trabectedin-treated macrophages exhibited greater $[Ca^{2+}]_i$ in comparison to M0 macrophages ($n = 4$, $p < 0.01$, trabectedin 5 nM vs. resting). Similar results were observed when we compared LPS-stimulated vs. M0 macrophages, ($n = 5$, $p < 0.05$, LPS vs. resting). Fig. 3B shows the degree of thapsigargin-induced (TG) emptying of Ca^{2+} from the endoplasmic reticulum (ER) in each experimental condition in a 0 mM Ca^{2+} solution.

The bar chart represents the area under the curve obtained after emptying the ER stored-Ca^{2+}, in which it is shown that the Ca^{2+} emptying from M1 macrophages is lower than in resting macrophages. We also observed that macrophages treated with trabectedin stored more Ca^{2+} than the resting condition. The stored-operated calcium entry (SOCE) through the CRAC channels was induced by exchanging the 0 mM Ca^{2+} solution for the same solution containing Ca^{2+} (1.2 mM

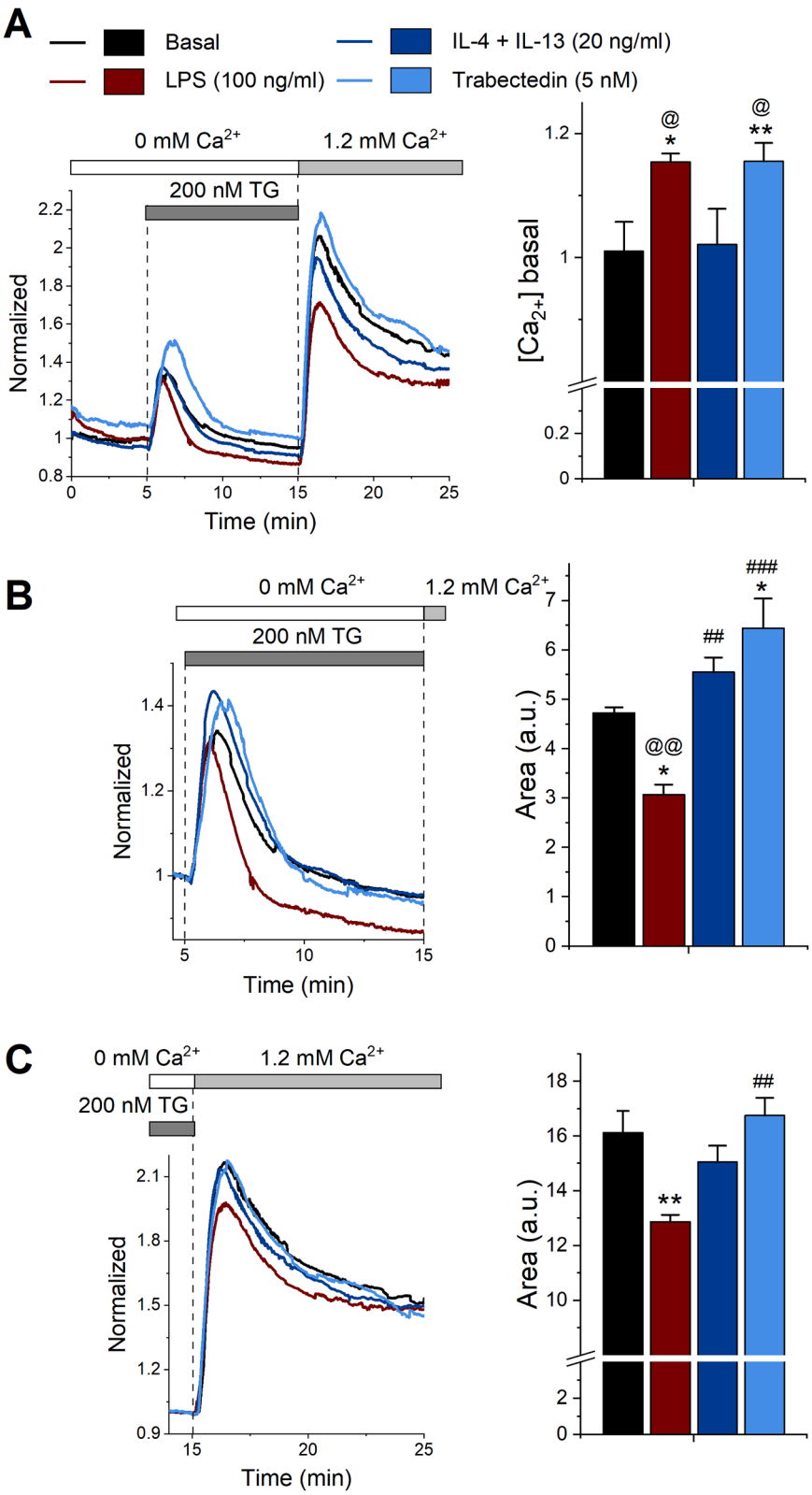

Fig. 3. Effects of trabectedin on Ca^{2+} movements in peritoneal macrophages. (A) Intensity of FLUO-4 and vs. elapsed time at different polarization states and. The emptying of Ca^{2+} stores stored in the ER was induced with thapsigargin (TG, 200 nM) in a 0 mM Ca^{2+} solution and it was analyzed as the area under the curve between 5 and 10 min of the experiment. Calcium influx into the cell (SOCE) through CRAC channels was induced by exchanging the 0 mM Ca^{2+} solution for the same one with 1.2 mM Ca^{2+} and was analyzed as the area under the curve between the 15–20 min of the experiment (n = 4–6). The bar diagram represents the basal concentration of Ca^{2+} inside the macrophages at the beginning of the experiment (n = 4–6). (B) Emptying of Ca^{2+} stores stored in the ER in different polarization states of macrophages. The normalized FLUO-4 fluorescence intensity is plotted versus elapsed time at 0 mM Ca^{2+} end of each condition. The mean of 4–6 experiments is shown. The diagram represents the release of Ca^{2+} from the ER after stimulation with TG (200 nM) (n = 4–6). (C) Ca^{2+} entry through CRAC channels in different polarization states of macrophages. Normalized FLUO-4 fluorescence intensity is plotted against steady-state fluorescence intensity at the end of each condition after stimulation with TG (n = 4–6). The diagram represents the SOCE current (n = 4–6). * $p < 0.05$, ** $p < 0.01$, *** $p < 0.001$ vs. rest; # $p < 0.05$, ## $p < 0.01$, ### $p < 0.001$ vs. LPS (100 ng/ml); @ $p < 0.05$, @ @ $p < 0.01$, vs. IL4 & IL-13 (20 ng/ml) (ANOVA and Test-Tukey).

Ca^{2+}). Fig. 3C shows the SOCE in each of the experimental conditions. The bar chart represents the area under the curve generated after the change in fluorescence intensity of FLUO-4 when Ca^{2+} enters from the outside into the macrophages. Only the LPS-stimulated macrophages exhibited a lower SOCE than the rest of the experimental conditions ($p < 0.01$ in LPS ng/ml 100 vs. M0 macrophages). Considering the decrease observed in *Stim1* mRNA levels (ER Ca^{2+} sensor) in trabectedin 5 nM-treated macrophages (Fig. 2J), we expected that, in trabectedin-treated macrophages, SOCE would be lower than in resting ones since the opening of the ORAI1 channels (whose expression is not compromised), requires interaction with STIM1.

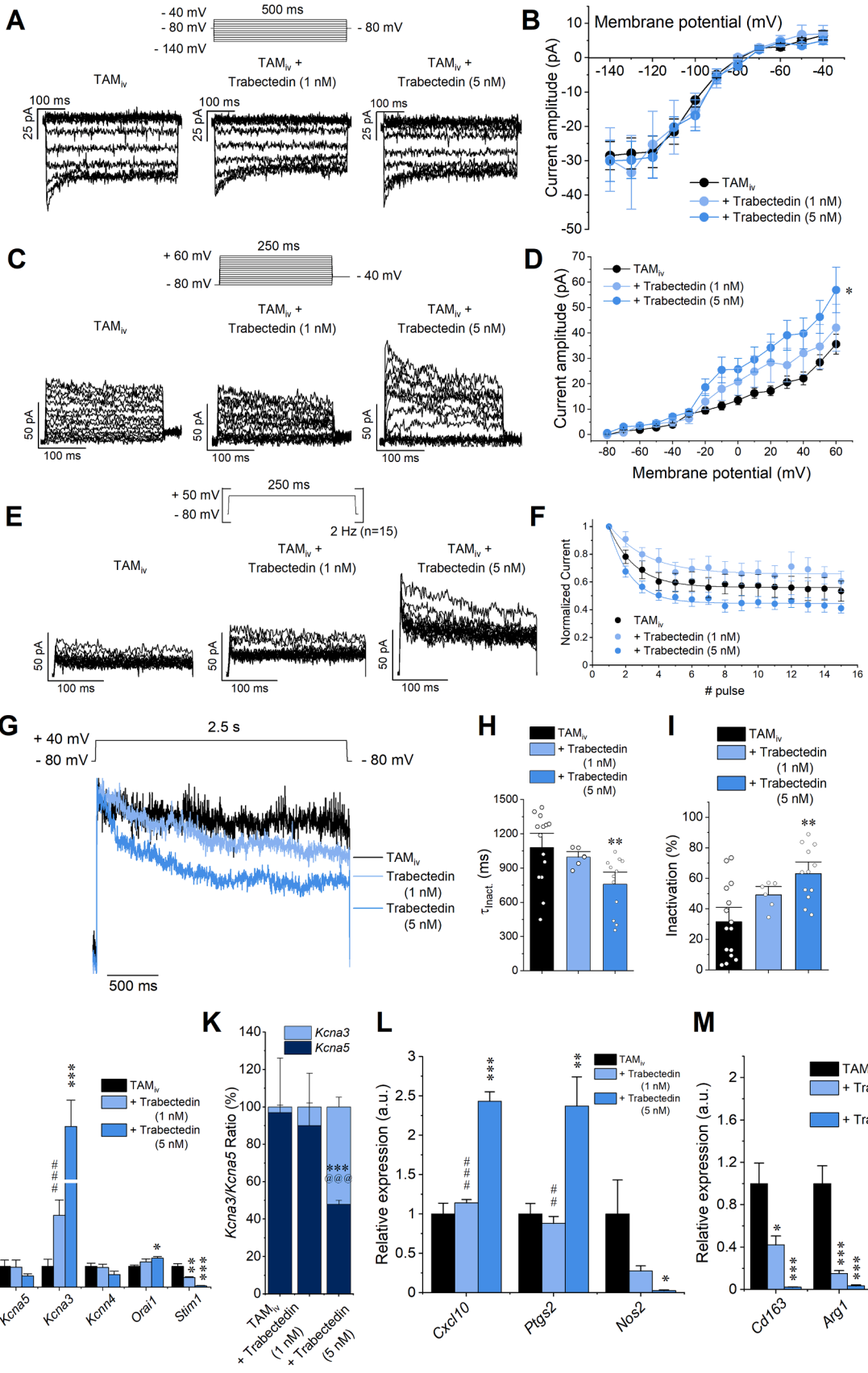

(caption on next page)

Fig. 4. Effects of trabectedin (1, 5 and 100 nM) on K_{ir} and K_v in TAM_{iv}. Levels of expression of ion channels and also on M1 and M2 markers in TAM_{iv}. Effects of trabectedin on K^+ currents recorded from TAM_{iv}. (A) Records of I_{K1} current from TAM_{iv} macrophages in the absence and in the presence of trabectedin, after applying the pulse protocol shown. (B) I-V ratio of I_{K1} obtained after measuring the amplitude of the current at the end of the records shown in panel A (n = 8–26). (C) Records of the K_V current from TAM_{iv} macrophages in the absence and in the presence of trabectedin, after applying the pulse protocol shown. (D) I-V relationship of the K_V currents obtained after measuring the amplitude of the current at the end of the records shown in panel C (n = 18–38). (E) Representative records of K_V currents from TAM_{iv} in the absence and in the presence of trabectedin, obtained after applying the pulse train shown in the upper part. (F) Use-dependence of K_V current shown in panel E, after normalizing the maximum amplitude of each trace to the maximum current amplitude generated during the application of the train of pulses versus pulse number (n = 11–24). (G) Representative records of TAM_{iv} in the absence and in the presence of trabectedin, obtained after applying the long depolarizing pulse of 2.5 s shown in the upper part. (H) Inactivation time constant (τ_{Inact}) obtained after fitting the traces shown in panel G to a monoexponential function (n = 12–30), and (I) Degree of current inactivation produced by the application of depolarizing pulses of 2.5 s applied to TAM_{iv} in the absence and in the presence of trabectedin (n = 14–30). ** $p < 0.01$ (1-way ANOVA, followed by a Test-Tukey). (J) RT-qPCR of the genes of different ion channels in TAM_{iv} in the absence and in the presence of trabectedin (n = 3–9). (K) Expression ratio of $K_V1.5$ and $K_V1.3$ measured by RT-qPCR (n = 3–11). (L) RT-qPCR of the proinflammatory genes (*Cxcl10*, *Ptgs2* and *Nos2*) in TAM_{iv} in the absence and in the presence of trabectedin (n = 4–9). (M) RT-qPCR of the anti-inflammatory genes (*CD163*, *Arg1* and *Hmox1*) in TAM_{iv} in the absence and in the presence of trabectedin (n = 3–9). * $p < 0.05$, ** $p < 0.01$, *** $p < 0.001$ vs. rest; # $p < 0.05$, ## $p < 0.01$ vs. TAM_{iv} (48 h) (1-way ANOVA, followed by a Test-Tukey).

3.4. Trabectedin and K^+ currents of in vitro generated tumor-associated macrophages (TAM_{iv})

We generated TAM_{iv} co-culturing resting macrophages with the ID8 tumor cell line for 48 h. The K_{ir} and K_V currents elicited in TAM_{iv} exhibited similar amplitudes to those recorded in M2 polarized macrophages with IL-4 + IL-13 (Supplementary Fig. 1), suggesting that TAM_{iv} exhibits an anti-inflammatory phenotype.

The amplitude of the Kir current obtained in the TAM_{iv} was not modified after the treatment with sub-cytotoxic concentrations of trabectedin (Fig. 4A-B). Fig. 4C-D shows that only the highest sub-cytotoxic trabectedin concentration (5 nM) increased the K_V amplitude of this current. These data seem to indicate that the anti-inflammatory phenotype exhibited by TAM_{iv} requires higher concentrations of trabectedin to produce the same effect observed in resting macrophages and thus re-educate TAM_{iv} towards a pro-inflammatory phenotype (Supplementary Fig. 4). The small increase in the amplitude of the K_V current produced by trabectedin (5 nM) in TAM_{iv} could also be due to an increase in the expression of the $K_V1.3$ channels. To check this, we applied a pulse train Fig. 4E) and after normalizing we obtained the use dependency of each experimental condition (Fig. 4E-F). K_V currents generated by trabectedin-treated TAM_{iv} exhibited the same degree of use-dependent decay as the untreated TAM_{iv} (n = 8–15, $p > 0.05$ vs. untreated TAM_{iv}). However, the depolarizing pulse of 2.5 s showed differences between the different experimental groups. The inactivation kinetics of the current traces obtained in TAM_{iv} + trabectedin (1 nM) were not modified compared to untreated TAM_{iv} (n = 6–14, $p > 0.05$) (Fig. 4G-H). Trabectedin (1 nM) was also unable to modify the inactivation percentage of the K_V current (n = 6–16, $p > 0.05$) (Fig. 4G and I). However, treatment of TAM_{iv} with the highest sub-cytotoxic concentration used accelerated the τ_{Inac} compared to untreated TAM_{iv} (n = 12–14, $p < 0.01$) (Fig. 4G-H) and also increased the percentage of K_V current inactivation compared to untreated TAM_{iv} (n = 12–16, $p < 0.01$) (Fig. 4G and I). These changes in the electrophysiological characteristics of the K_V currents recorded in trabectedin 5 nM-treated TAM_{iv} are due to an increase in the relative expression of *Kcna3* (Fig. 4J) and, therefore, to a change in the $K_V1.3/K_V1.5$ ratio of the hetero-tetramers that generate the K_V current of the TAM_{iv} (Fig. 4K). These data suggest that TAM_{iv}, which have an anti-inflammatory phenotype, requires a higher concentration of trabectedin to increase the amplitude of the K_V current, because of the increase in the expression of the $K_V1.3$ channels. At the same time, trabectedin increased the mRNA levels of the *Cxcl10* and *Ptgs2* pro-inflammatory markers in TAM_{iv} (Fig. 4L) and decreased the *Cd163*, *Arg1* and *Hmox1* anti-inflammatory markers (Fig. 4M). Thus, trabectedin changes the anti-inflammatory phenotype of TAM_{iv} not only at the electrophysiological, but also at the molecular level.

3.5. Characterization of K^+ ion currents of tumor-associated macrophages

TAMs obtained from tumor-bearing mice exhibited a low amplitude and very noisy K_V current, both in TAMs from untreated and trabectedin-treated tumor-bearing mice (TAMs Treated) (Fig. 5A). Fig. 5B shows that the K_V current obtained in the TAMs exhibited a greater amplitude than that recorded in the TAMs obtained from trabectedin-treated mice (n = 10, $p < 0.05$). Because it is known that macrophages express K_{Ca} channels, we recorded the K_{Ca} current using an [10^{-6} M $Ca^{2+}]_i$ internal solution. Thus, we recorded a Ca^{2+}-dependent K^+ current with slower activation kinetics than the activation kinetics of the K_V current. The K_{Ca} current records obtained in TAMs show faster activation kinetics than those from TAMs from trabectedin-treated mice (Fig. 5C). K_{Ca} records under both experimental conditions show a slight inactivation of the current during the application of depolarizing pulses, and an accumulation of the inactivation in the current records obtained from TAMs from untreated mice. These data suggest that TAMs have a mixture of K_V and K_{Ca} currents and also that the current recorded in the TAMs Treated is mainly due to K_{Ca} channels. The K_{Ca} current amplitude at the end of the 250 ms depolarizing pulses was greater in the TAMs Treated than in the TAMs (n = 4–6, $p < 0.05$) (Fig. 5D). These changes in the electrophysiological characteristics of the K^+ currents recorded in TAMs from treated mice are due to a decrease in the relative expression of *Kcna3* (Fig. 5E) and also to an increase in *Kcnn4*, which led to a phenotype more similar to $K_{Ca}3.1$ in TAMs from treated mice (Fig. 5E). These results might indicate that, unlike what was observed in TAM_{iv}, the main K^+ current in TAMs is the K_{Ca} current with a small contribution from the K_V current. Furthermore, treatment with trabectedin in tumor-bearing mice appears to change the type of K^+ ion current exhibited by TAMs, with greater importance on the K_{Ca} current.

Using the [10^{-9} M $Ca^{2+}]_i$ internal solution we observed that the K_V current records of both TAMs situations also showed an inward current at the start of the depolarizing pulses of 250 ms duration (Fig. 5A). After applying the ramp shown in the upper part of Fig. 5F and using an internal solution [10^{-9} M $Ca^{2+}]_i$, a current inward current was obtained in both TAMs. These current records obtained seem to indicate that the inward current is slightly higher in TAMs Treated than in TAMs. Indeed, when we measured the amplitude of the current between 25 and 50 ms of the depolarizing pulse, we observed that the inward current has a greater amplitude in the TAMs Treated than in the TAMs (n = 8, $p < 0.05$) (Fig. 5G). We ruled out that the input current was due to an L-type Ca^{2+} channel because it was not inhibited after perfusing macrophages with Co^{2+} (2 mM) in the external solution (Fig. 5H). In addition, Ni^{2+} (50 μM) was used in the external solution and, unfortunately, the small amplitude of this inward current did not allow us to analyze the possible effects of Ni^{2+}, since at this concentration Ni^{2+} displaces the activation curve of the Ca^{2+} T-type channels (Fig. 5I). Finally, when we added to the external solution La^{3+} (100 μM), the inward current was completely inhibited (Fig. 5J). Similarly, we also observed that this

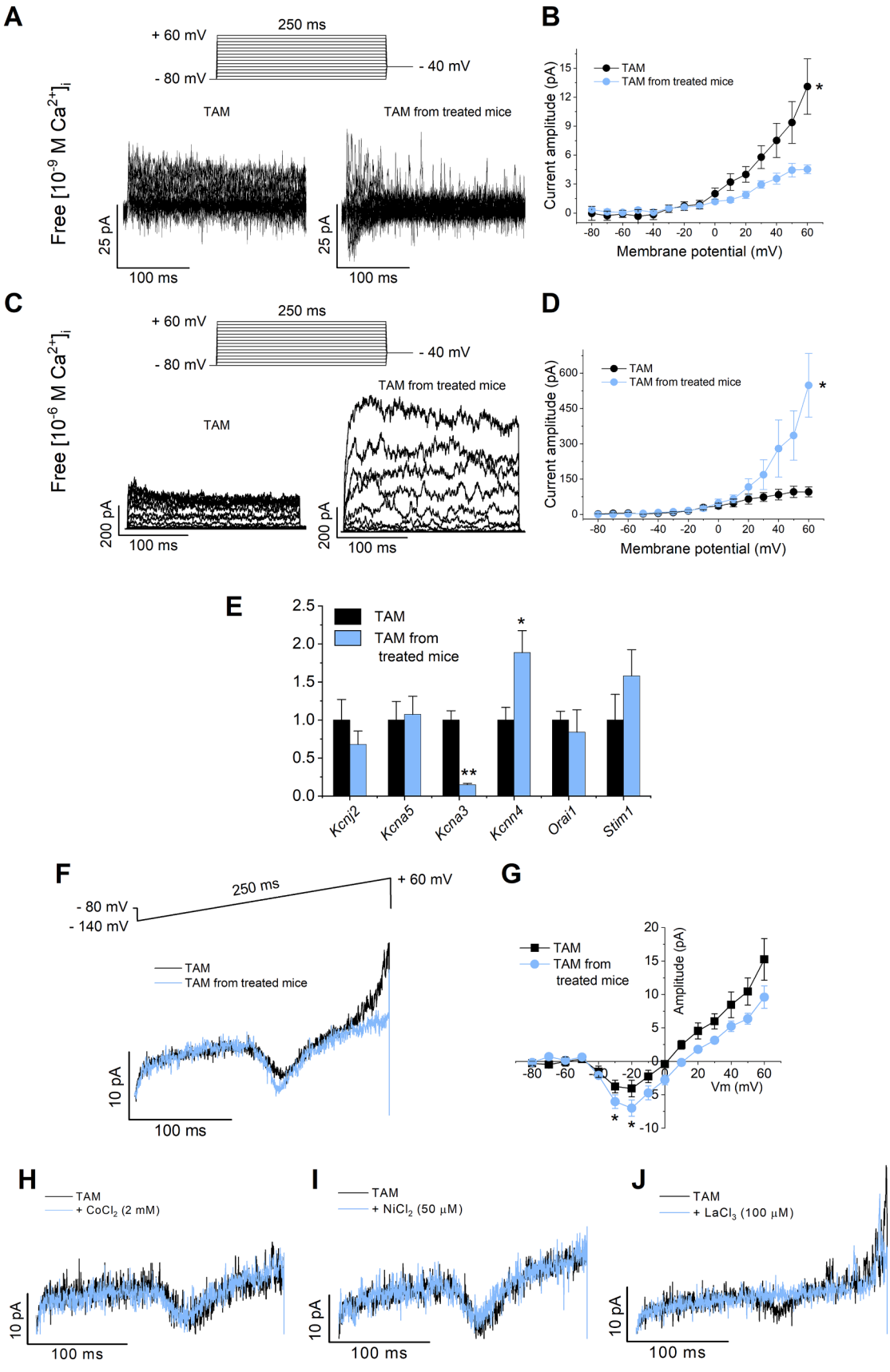

(caption on next page)

Fig. 5. Characteristics of TAM from control mice and TAM from treated mice on K currents. Characterization of an inward current. (A) Representative recordings of TAMs obtained from tumor-bearing mice untreated or treated with trabectedin, obtained after applying the pulse protocol shown above and using an internal solution with a concentration of free Ca^{2+} of 10^{-9} M. (B) I-V relationship of K_V current of untreated or trabectedin-treated TAM under these experimental conditions (n = 8). (C) Representative records of the K_V current of TAM and TAM-trabectedin treated mice, obtained after applying the pulse protocol shown in the upper part and using an internal solution with a free Ca^{2+} concentration of 10^{-6} M. (D) I-V relationship of K_V currents from TAM and TAM-trabectedin treated under these experimental conditions (n = 5–9). (E) Expression ratio of ion channels measured by RT-qPCR (n = 3–11). (F) Current recordings generated in TAM from tumor-naïve or trabectedin-treated mice obtained after applying the ramp shown in the upper panel (n = 3). (G) I-V relationship of the K_V current measured between 25 and 50 ms, obtained after applying depolarizing pulses of 250 ms duration from − 80 mV to + 60 mV in increments of 10 mV at a frequency of 0.02 Hz. (H) Current records generated in TAM in the absence and in the presence of $CoCl_2$ (2 mM), $NiCl_2$ (50 μM) (I) or $LaCl_3$ (100 μM) (J).

inward current was inhibited when the holding potential was set at − 40 mV and depolarizing pulses of 250 ms duration were applied from − 80 mV to + 60 mV in increments of 10 mV (Data not shown). Taken together, these data allow us to suggest that the inward current present in TAMs may be due to TRP channel activity since they are sensitive to La^{3+}. However, we cannot rule out the possibility that it is due to the activity of Ca^{2+} T-type channels, since these Ca^{2+} channels are also sensitive to La^{3+}, and also because they are inactivated with a holding potential of − 40 mV.

3.6. K^+ ion currents of peritoneal macrophages from tumor-bearing mice treated or not with trabectedin

Finally, we studied the K^+ ion currents present on peritoneal macrophages from tumor-bearing mice that were treated or not with trabectedin (tumor peritoneal macrophages or T-PMs). As shown, the amplitude of the I_{K1} currents recorded in the T-PMs from tumor-bearing mice treated or not with trabectedin was similar (n = 6–12, $p > 0.05$). However, both exhibited an I_{K1} current of smaller amplitude than the I_{K1} current registered in resting macrophages (n = 26, $p < 0.001$) (Fig. 6A-B). The amplitude of the K_V current recorded in the T-PMs was greater than that recorded in the resting macrophages (n = 7–38, $p < 0.001$) (Fig. 6C-D). The results of the I_{K1} and K_V currents recorded in T-PMs indicate an electrophysiological phenotype of pro-inflammatory macrophages. In trabectedin-treated tumor-bearing mice, the K_V current had a smaller amplitude than that observed in T-PMs (n = 7–13; $p < 0.001$) (Fig. 6C-D), indicating that trabectedin exhibits an inhibitory effect on the immunosuppressive environment, not an anti-inflammatory effect as such (it would favor M1, thus it has an anti-tumor effect because it favors anti-tumor inflammation).

The use-dependent decay of the K_V channels in T-PMs was greater than that observed in resting macrophages (n = 6–24, $p < 0.001$) (Fig. 6E-F). However, the use-dependent decay observed in the T-PMs Treated was similar to that of the T-PMs (n = 6–11, $p > 0.05$) (Fig. 6E-F). Similar results were obtained after applying a depolarizing pulse of 2.5 s duration at + 40 mV (Fig. 6G). The inactivation kinetics of K_V current were unchanged in T-PMs after treatment of the tumor-bearing mice with trabectedin (n = 4–8; $p > 0.05$) (Fig. 6G-H). However, this inactivation process was accelerated compared to the resting macrophages ($p < 0.05$) (Fig. 6G-H). The K_V current degree of inactivation was greater in T-PMs and in T PMs Treated than in resting macrophages (n = 4–10, $p < 0.05$) and, therefore, treatment with trabectedin did not modify this parameter (Fig. 6I).

If we consider the relative expression of the *Kcna3* mRNA, we observe that it increased in the T-PMs and in the treated T-PMs, which explains the increase in the amplitude of the K_V current that we have observed in these macrophages vs. those recorded in resting macrophages (Fig. 6J). Likewise, there was an increase in the expression levels of the *Kcna5* mRNA in the treated T-PMs, which, in turn, is different from the level of *Kcna5* expression that present T-PMs. The increase in $K_V1.5$ channels could explain the decrease in the amplitude of the K_V current obtained in T-PMs Treated, which produces a change in the $K_V1.3/K_V1.5$ ratio of the heterotetramers that generate macrophage current K_V (Fig. 6K). Furthermore, the relative levels of mRNA of the pro-inflammatory markers *Cxcl10*, *Ptgs2* and *Nos2* are increased in T-PMs compared to those of resting macrophages (Fig. 6L). These data also showed that T-PMs show a pro-inflammatory phenotype, although it should be noted that certain anti-inflammatory markers such as *Arg1* and *Hmox1* are elevated (Fig. 6M). Trabectedin treatment of tumor-bearing mice decreased the expression of the pro-inflammatory markers *Cxcl10*, *Ptgs2* and *Nos2* in the T-PMs (Fig. 6L). All these data suggest that trabectedin exerts an inhibitory effect on the immunosuppressive milieu.

4. Discussion

In the present study, we have characterized the electrophysiological effects of trabectedin on murine peritoneal macrophages, TAM_{iv}, TAMs and peritoneal macrophages from tumor-bearing mice treated or non-treated with this drug. Our data demonstrate that: 1) trabectedin-treatment of peritoneal macrophages changes their electrophysiology, due to changes in the expression of K^+ channels, as well as changes in M1 and M2 markers. 2) trabectedin-treatment of TAM_{iv} also modified their electrophysiology, but to a lesser extent; in parallel with modifications with M1 and M2 markers. 3) TAMs isolated from tumors generated in mice exhibited a K^+ current that is a mixture of K_V and K_{Ca}. 4) Trabectedin-treated TAMs mostly exhibited a K^+ current elicited by K_{Ca} channels. From all these features, we conclude that the anti-tumor effect of trabectedin is not only due to its effects on tumor cells, but also to the modulation of the tumor microenvironment, due, at least in part, to the modulation of the polarization of the macrophages present in the tumor.

Previous reports demonstrated that trabectedin induces apoptosis [41]. In this study, similar results were observed. Activation, mostly M1, of peritoneal macrophages increased their resistance to trabectedin. Trabectedin, at sub-cytotoxic concentrations within its therapeutic range [42], did not modify: i) the viability of macrophages, ii) ROS production or iii) the mitochondrial $\Delta\psi$.

Our results indicate that trabectedin does not produce direct effects on $K_V1.3$ or $K_V1.5$ channels. However, incubation of resting peritoneal macrophages or TAM_{iv} with sub-cytotoxic concentrations of trabectedin induces M1-like polarization, observed both in their electrophysiology and in the M1 and M2 markers. In basal peritoneal macrophages we observed: i) a decrease in I_{K1}, as a consequence of a downregulation of the expression of *Kcnj2*, and ii) an increase of the K_V current, due to an increase in the expression of *Kcna3*, accompanied by an increase in the $K_V1.3$ protein expression, without modifications in the expression of *Kcna5*, which leads to an increase in the $K_V1.3/K_V1.5$ ratio of heterotetrameric K_V channels. The variation in the stoichiometry of K_V heterotetramers was reflected in their electrophysiology. Thus, the slight cumulative inactivation observed in resting macrophages and in TAM_{iv} increased in macrophages incubated with sub-cytotoxic concentrations of trabectedin. All these results show that trabectedin modulates the state of polarization of macrophages towards a pro-inflammatory phenotype and also that the required sub-cytotoxic concentration varies depending on the state of polarization in which they are found (greater for TAM_{iv} than for resting).

We also observed that sub-cytotoxic concentrations of trabectedin not only increased the expression of M1 markers in resting macrophages and TAM_{iv}, but also decreased the expression of anti-inflammatory markers. The decrease in M1 markers in T-PM with a pro-inflammatory phenotype confirms that trabectedin attenuates the

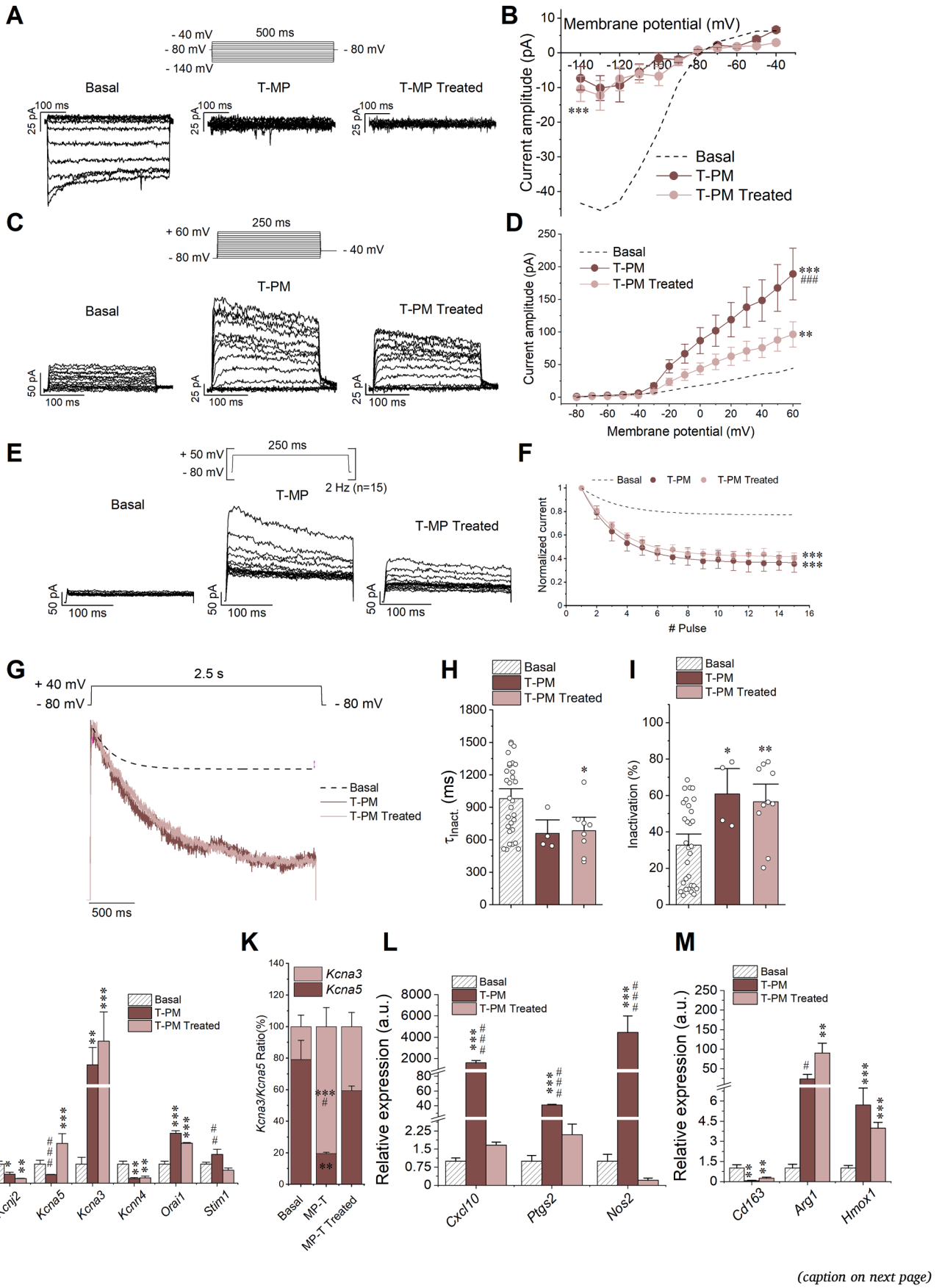

(caption on next page)

Fig. 6. Characteristics of peritoneal macrophages obtained from tumor-bearing mice non-treated (MP-T) or tumor-bearing mice treated with trabectedin (MP-T Treated). (A) Representative recordings of I_{K1} from MP-T or MP-T Treated, obtained after applying the pulse protocol shown. (B) I-V relationship of I_{K1} from PM-T and PM-T Treated. The dashed line shows the I-V relationship of I_{K1} from Resting macrophages (n = 5–12). (C) Representative records of K_V current of PM-T and PM-T Treated, obtained after applying the pulse protocol shown. (D) I-V relationship of K_V currents of PM-T and PM-T Treated. The dashed line shows the I-V relationship of the K_V current of Resting macrophages (n = 7–13). (E) Representative records of MP-T and MP-T Treated, obtained after applying the pulse train shown. (F) Use-dependence of the PM-T and PM-T Treated, after normalizing the maximum amplitude of the current of the pulse train against the number of pulse. The dashed line shows the use-dependency of Resting macrophages (n = 6–11). (G) Representative records of PM-T and PM-T Treated, obtained after applying the pulse protocol shown. The dashed line shows a record from a resting macrophage after applying the same protocol. (H) Time-constant of inactivation (τ_{Inact}) obtained after fitting the current trace shown in panel G to a monoexponential function (n = 4–8). (I) Degree of inactivation obtained in traces shown in panel G (n = 4–10). (J) RT-qPCR of the genes of different ion channels in resting macrophages, in MP-T and MP-T Treated (n = 4–9) (K) Expression ratio of $K_V1.5$ and $K_V1.3$ measured by RT-qPCR. (L) RT-qPCR of proinflammatory genes in resting, MP-T and Treated MP-T macrophages (n = 3–9). (M) RT-qPCR of anti-inflammatory genes in resting macrophages, the MP-T and MP-T Treated (n = 3–9). Statistical analysis: * $p < 0.05$, ** $p < 0.01$, *** $p < 0.001$ vs. rest; # $p < 0.05$, ## $p < 0.01$, ### $p < 0.001$ vs. MP-T Treated (ANOVA and Test-Tukey).

inflammatory response without losing the anti-tumor phenotype. This variation in the expression of M1 markers produced by sub-cytotoxic concentrations of trabectedin reinforces the close relationship between ionic currents and signaling pathways, showing that trabectedin modulates macrophages differently, depending on their functional state of polarization. ROS production induced by trabectedin in macrophages may be due to the dysfunction of mitochondrial respiration [43,44], which we detected in the different polarization states, after inducing apoptosis. While pro-inflammatory macrophages produce a large amount of ROS, anti-inflammatory macrophages (M2) require high concentrations of trabectedin to produce it; suggesting again that trabectedin acts differently depending on the polarization of macrophages.

Surprisingly, peritoneal macrophages from tumor-bearing mice exhibited a pro-inflammatory phenotype. Like LPS-stimulated macrophages, T-PM exhibited: i) an I_{K1} of very small amplitude, likely due to a decrease in the expression of *Kcnj2*; and ii) a greater amplitude K_V current compared to peritoneal macrophages from control mice, due to a higher $K_V1.3/K_V1.5$ ratio of K_V heterotetramers, due to an increase in the expression of *Kcna3*. Treatment of these immunosuppressed mice with trabectedin changed the expression pattern of the ion channels of their peritoneal macrophages. The $K_V1.3/K_V1.5$ ratio of their heterotetrameric K_V channels decreased, likely due to an increase in the expression of *Kcna5* without changes in the relative expression of *Kcna3*. This increase in *Kcna5* gene expression could explain the decrease in the total K_V current, since it has been demonstrated that $K_V1.5$ impairs $K_V1.3$ surface expression [45].

A joint suppression of *Stim1* and *Stim2* may result in SOCE inhibition [5,46–49]. This could be the reason that the decrease in *Stim1* observed in trabectedin-treated resting macrophages did not produce consequences in SOCE. The correct signaling of intracellular Ca^{2+} is essential for the accurate function of macrophages, mediated by other transporters or ion channels that measure Ca^{2+} conductance and induce the release of stored Ca^{2+} deposits [5,50,51]. We have registered in TAMs an inward ion current that may be due to TRP channel activity since they are sensitive to La^{3+}, although we cannot rule out the possibility that it should be a Ca^{2+} T-type channel, since they are also sensitive to La^{3+} and they are inactivated with a holding potential of − 40 mV.

At the tumor microenvironment level, the anti-tumor ability of trabectedin is due, at least in part, to its ability to modulate the state of polarization of TAM_{iv} towards a pro-inflammatory phenotype. TAMs treated or not with trabectedin, exhibited different electrophysiological characteristics to those generated in vitro. However, trabectedin also induced changes in the expression pattern of ion channels in TAMs. On the other hand, while in TAM_{iv} an increase in the $K_V1.3/K_V1.5$ ratio was observed due to an increase in the expression of *Kcna3*; the electrophysiology of TAMs is different, the K_{Ca} current contribution being greater than K_V current to maintain the E_m. These dissimilarities between the expression of ion channels in both kinds of macrophages may suggest that may depend on the embryonic origin of the macrophages. Indeed, TAM_{iv} are generated from embryonic precursors derived from the yolk sac; whereas TAMs come from mononuclear cell precursors that circulate through the bloodstream attracted to the tumor microenvironment by both released cytokines by tumor cells as well as by T lymphocytes [52–54].

In summary, we conclude that the anti-tumor capacity of trabectedin is not only due to its effects on tumor cells, but also to the modulation of the tumor microenvironment, due, at least in part, to the modulation of the polarization of the macrophages present in the tumor, varying the expression of different macrophage ion channels.

Funding

This research was funded by AEI, Grants SAF2016-75021-R (to CV) funded by MICIN/AEI/10.13039/501100011033 and by "ERDF A way of making Europe"; Grants PID2019-104366RB-C21 (to CV) and PID2020-113238RB-I00 (to L.B.) funded by MCIN/AEI/10.13039/501100011033; by CIBERCV, Grant CB/11/00222 funded by Instituto de Salud Carlos III (to LB and CV) co-financed by the European Development Regional Fund "A Way to Achieve Europe"); Comunidad de Madrid Programa Biociencias (P2022-BMD-7223); by CSIC Grants PIE201820E104 and 2019AEP148 (to CV). This research was partially funded by a grant from a PharmaMar S.A. Grant.

Ethics approval and consent to participate

The Institutional Ethics Committee (PROEX 197/18) approved the animal studies performed in this article. All animal procedures conformed to EU Directive 2010/63 and Recommendation 2007/526/EC regarding the protection of animals used for experimental and other scientific purposes, enforced in Spanish law (RD 53/2013). C57BL/6J male mice were housed under controlled conditions at 25 °C in 12-hour light/dark cycles with ad libitum access to water and food in an environment with maintained temperature and relative humidity.

CRediT authorship contribution statement

D.A.P. designed the study, performed experiments, designed and performed experiments, analyzed data, designed the figures and wrote the first draft of the manuscript. A.P.-R. and M.M. provided experimental and intellectual input. A.B.G.-R. and P.M.A. provided biological samples. L.B. provided intellectual input and revised the manuscript. C. V. designed the project, wrote the paper, provided funding and intellectual input and organized the information.

Conflict of interest statement

P.M.A. is an employee of PharmaMar. The authors declare to have received a grant from PharmaMar S.A. to support in part the costs of the research. Trabectedin was provided by PharmaMar S.A. This funder had no role in the design of the study; analyses and interpretation of data; in the writing of the manuscript; or in the decision to publish the results.

Acknowledgments

The authors thank the services of microscopy and genomics from the Institute of Biomedical Research Alberto Sols, for technical support.

Consent for publication

All authors concur and approve the submission of the manuscript.

Appendix A. Supplementary material

Supplementary data associated with this article can be found in the online version at doi:10.1016/j.biopha.2023.114548.

References

[1] S. Feske, H. Wulff, E.Y. Skolnik, Ion channels in innate and adaptive immunity, Annu. Rev. Immunol. 33 (2015) 291–353, https://doi.org/10.1146/annurev-immunol-032414-112212.
[2] P.J. Hanley, B. Musset, V. Renigunta, S.H. Limberg, A.H. Dalpke, R. Sus, K.M. Heeg, R. Preisig-Muller, J. Daut, Extracellular ATP induces oscillations of intracellular Ca2+ and membrane potential and promotes transcription of IL-6 in macrophages, Proc. Natl. Acad. Sci. USA 101 (25) (2004) 9479–9484, https://doi.org/10.1073/pnas.0400733101.
[3] C. Moreno, P. Prieto, A. Macias, M. Pimentel-Santillana, A. de la Cruz, P.G. Traves, L. Bosca, C. Valenzuela, Modulation of voltage-dependent and inward rectifier potassium channels by 15-epi-lipoxin-A4 in activated murine macrophages: implications in innate immunity, J. Immunol. 191 (12) (2013) 6136–6146, https://doi.org/10.4049/jimmunol.1300235.
[4] S. Srivastava, P. Choudhury, Z. Li, G. Liu, V. Nadkarni, K. Ko, W.A. Coetzee, E. Y. Skolnik, Phosphatidylinositol 3-phosphate indirectly activates KCa3.1 via 14 amino acids in the carboxy terminus of KCa3.1, Mol. Biol. Cell 17 (1) (2006) 146–154, https://doi.org/10.1091/mbc.e05-08-0763.
[5] M. Vaeth, I. Zee, A.R. Concepcion, M. Maus, P. Shaw, C. Portal-Celhay, A. Zahra, L. Kozhaya, C. Weidinger, J. Philips, D. Unutmaz, S. Feske, Ca2+ signaling but not store-operated Ca2+ entry is required for the function of macrophages and dendritic cells, J. Immunol. 195 (3) (2015) 1202–1217, https://doi.org/10.4049/jimmunol.1403013.
[6] N. Villalonga, M. David, J. Bielanska, R. Vicente, N. Comes, C. Valenzuela, A. Felipe, Immunomodulation of voltage-dependent K+ channels in macrophages: molecular and biophysical consequences, J. Gen. Physiol. 135 (2) (2010) 135–147, https://doi.org/10.1085/jgp.200910334.
[7] R. Vicente, A. Escalada, M. Coma, G. Fuster, E. Sanchez-Tillo, C. Lopez-Iglesias, C. Soler, C. Solsona, A. Celada, A. Felipe, Differential voltage-dependent K+ channel responses during proliferation and activation in macrophages, J. Biol. Chem. 278 (47) (2003) 46307–46320, https://doi.org/10.1074/jbc.M304388200.
[8] R. Vicente, A. Escalada, N. Villalonga, L. Texido, M. Roura-Ferrer, M. Martin-Satue, C. Lopez-Iglesias, C. Soler, C. Solsona, M.M. Tamkun, A. Felipe, Association of Kv1.5 and Kv1.3 contributes to the major voltage-dependent K+ channel in macrophages, J. Biol. Chem. 281 (49) (2006) 37675–37685, https://doi.org/10.1074/jbc.M605617200.
[9] H. Wulff, R. Kohler, Endothelial small-conductance and intermediate-conductance KCa channels: an update on their pharmacology and usefulness as cardiovascular targets, J. Cardiovasc. Pharmacol. 61 (2) (2013) 102–112, https://doi.org/10.1097/FJC.0b013e318279ba20.
[10] E.K. Gallin, Ion channels in leukocytes, Physiol. Rev. 71 (3) (1991) 775–811, https://doi.org/10.1152/physrev.1991.71.3.775.
[11] I. Jou, H. Pyo, S. Chung, S.Y. Jung, B.J. Gwag, E.H. Joe, Expression of Kv1.5 K+ channels in activated microglia in vivo, Glia 24 (4) (1998) 408–414.
[12] Y. Kubo, T.J. Baldwin, Y.N. Jan, L.Y. Jan, Primary structure and functional expression of a mouse inward rectifier potassium channel, Nature 362 (6416) (1993) 127–133, https://doi.org/10.1038/362127a0.
[13] T. Schilling, C. Stock, A. Schwab, C. Eder, Functional importance of Ca2+-activated K+ channels for lysophosphatidic acid-induced microglial migration, Eur. J. Neurosci. 19 (6) (2004) 1469–1474, https://doi.org/10.1111/j.1460-9568.2004.03265.x.
[14] H. Wulff, A. Kolski-Andreaco, A. Sankaranarayanan, J.M. Sabatier, V. Shakkottai, Modulators of small- and intermediate-conductance calcium-activated potassium channels and their therapeutic indications, Curr. Med. Chem. 14 (13) (2007) 1437–1457, https://doi.org/10.2174/092986707780831186.
[15] Y.D. Gao, P.J. Hanley, S. Rinne, M. Zuzarte, J. Daut, Calcium-activated K(+) channel (K(Ca)3.1) activity during Ca(2+) store depletion and store-operated Ca(2+) entry in human macrophages, Cell Calcium 48 (1) (2010) 19–27, https://doi.org/10.1016/j.ceca.2010.06.002.
[16] S. Akira, K. Takeda, Toll-like receptor signalling, Nat. Rev. Immunol. 4 (7) (2004) 499–511, https://doi.org/10.1038/nri1391.
[17] S. Gordon, The macrophage: past, present and future, Eur. J. Immunol. 37 (Suppl. 1) (2007) S9–S17, https://doi.org/10.1002/eji.200737638.
[18] S. Gordon, F.O. Martinez, Alternative activation of macrophages: mechanism and functions, Immunity 32 (5) (2010) 593–604, https://doi.org/10.1016/j.immuni.2010.05.007.
[19] C. Pasare, R. Medzhitov, Control of B-cell responses by Toll-like receptors, Nature 438 (7066) (2005) 364–368, https://doi.org/10.1038/nature04267.
[20] S.K. Biswas, A. Mantovani, Macrophage plasticity and interaction with lymphocyte subsets: cancer as a paradigm, Nat. Immunol. 11 (10) (2010) 889–896, https://doi.org/10.1038/ni.1937.
[21] L.S. Ojalvo, W. King, D. Cox, J.W. Pollard, High-density gene expression analysis of tumor-associated macrophages from mouse mammary tumors, Am. J. Pathol. 174 (3) (2009) 1048–1064, https://doi.org/10.2353/ajpath.2009.080676.
[22] P.G. Traves, A. Luque, S. Hortelano, Macrophages, inflammation, and tumor suppressors: ARF, a new player in the game, Mediat. Inflamm. 2012 (2012), 568783, https://doi.org/10.1155/2012/568783.
[23] A. Mantovani, S. Sozzani, M. Locati, P. Allavena, A. Sica, Macrophage polarization: tumor-associated macrophages as a paradigm for polarized M2 mononuclear phagocytes, Trends Immunol. 23 (11) (2002) 549–555, https://doi.org/10.1016/s1471-4906(02)02302-5.
[24] G. Germano, R. Frapolli, C. Belgiovine, A. Anselmo, S. Pesce, M. Liguori, E. Erba, S. Uboldi, M. Zucchetti, F. Pasqualini, M. Nebuloni, N. van Rooijen, R. Mortarini, L. Beltrame, S. Marchini, I. Fuso Nerini, R. Sanfilippo, P.G. Casali, S. Pilotti, C. M. Galmarini, A. Anichini, A. Mantovani, M. D'Incalci, P. Allavena, Role of macrophage targeting in the antitumor activity of trabectedin, Cancer Cell 23 (2) (2013) 249–262, https://doi.org/10.1016/j.ccr.2013.01.008.
[25] B. Ruffell, L.M. Coussens, Macrophages and therapeutic resistance in cancer, Cancer Cell 27 (4) (2015) 462–472, https://doi.org/10.1016/j.ccell.2015.02.015.
[26] P.G. Santamaria, G. Moreno-Bueno, A. Cano, Contribution of epithelial plasticity to therapy resistance, J. Clin. Med. 8 (5) (2019), https://doi.org/10.3390/jcm8050676.
[27] K. Beatty, C. Winkelman, J.A. Bokar, P. Mazanec, Advances in oncology care: targeted therapies, ; quiz 335-6, AACN Adv. Crit. Care 22 (4) (2011) 323–334, https://doi.org/10.1097/NCI.0b013e3182310178.
[28] D. Duluc, M. Corvaisier, S. Blanchard, L. Catala, P. Descamps, E. Gamelin, S. Ponsoda, Y. Delneste, M. Hebbar, P. Jeannin, Interferon-gamma reverses the immunosuppressive and protumoral properties and prevents the generation of human tumor-associated macrophages, Int. J. Cancer 125 (2) (2009) 367–373, https://doi.org/10.1002/ijc.24401.
[29] G. Genard, A.C. Wera, C. Huart, B. Le Calve, S. Penninckx, A. Fattaccioli, T. Tabarrant, C. Demazy, N. Ninane, A.C. Heuskin, S. Lucas, C. Michiels, Proton irradiation orchestrates macrophage reprogramming through NFkappaB signaling, Cell Death Dis. 9 (7) (2018) 728, https://doi.org/10.1038/s41419-018-0757-9.
[30] C. Guiducci, A.P. Vicari, S. Sangaletti, G. Trinchieri, M.P. Colombo, Redirecting in vivo elicited tumor infiltrating macrophages and dendritic cells towards tumor rejection, Cancer Res. 65 (8) (2005) 3437–3446, https://doi.org/10.1158/0008-5472.CAN-04-4262.
[31] M.M. Kaneda, K.S. Messer, N. Ralainirina, H. Li, C.J. Leem, S. Gorjestani, G. Woo, A.V. Nguyen, C.C. Figueiredo, P. Foubert, M.C. Schmid, M. Pink, D.G. Winkler, M. Rausch, V.J. Palombella, J. Kutok, K. McGovern, K.A. Frazer, X. Wu, M. Karin, R. Sasik, E.E. Cohen, J.A. Varner, PI3Kgamma is a molecular switch that controls immune suppression, Nature 539 (7629) (2016) 437–442, https://doi.org/10.1038/nature19834.
[32] A. Mantovani, F. Marchesi, A. Malesci, L. Laghi, P. Allavena, Tumour-associated macrophages as treatment targets in oncology, Nat. Rev. Clin. Oncol. 14 (7) (2017) 399–416, https://doi.org/10.1038/nrclinonc.2016.217.
[33] C. Rolny, M. Mazzone, S. Tugues, D. Laoui, I. Johansson, C. Coulon, M.L. Squadrito, I. Segura, X. Li, E. Knevels, S. Costa, S. Vinckier, T. Dresselaer, P. Akerud, M. De Mol, H. Salomaki, M. Phillipson, S. Wyns, E. Larsson, I. Buysschaert, J. Botling, U. Himmelreich, J.A. Van Ginderachter, M. De Palma, M. Dewerchin, L. Claesson-Welsh, P. Carmeliet, HRG inhibits tumor growth and metastasis by inducing macrophage polarization and vessel normalization through downregulation of PlGF, Cancer Cell 19 (1) (2011) 31–44, https://doi.org/10.1016/j.ccr.2010.11.009.
[34] L. Sun, B. Chen, R. Jiang, J. Li, B. Wang, Resveratrol inhibits lung cancer growth by suppressing M2-like polarization of tumor associated macrophages, Cell Immunol. 311 (2017) 86–93, https://doi.org/10.1016/j.cellimm.2016.11.002.
[35] C. Belgiovine, E. Bello, M. Liguori, I. Craparotta, L. Mannarino, L. Paracchini, L. Beltrame, S. Marchini, C.M. Galmarini, A. Mantovani, R. Frapolli, P. Allavena, M. D'Incalci, Lurbinectedin reduces tumour-associated macrophages and the inflammatory tumour microenvironment in preclinical models, Br. J. Cancer 117 (5) (2017) 628–638, https://doi.org/10.1038/bjc.2017.205.
[36] M. D'Incalci, C.M. Galmarini, A review of trabectedin (ET-743): a unique mechanism of action, Mol. Cancer Ther. 9 (8) (2010) 2157–2163, https://doi.org/10.1158/1535-7163.MCT-10-0263.
[37] F. Grosso, R.L. Jones, G.D. Demetri, I.R. Judson, J.Y. Blay, A. Le Cesne, R. Sanfilippo, P. Casieri, P. Collini, P. Dileo, C. Spreafico, S. Stacchiotti, E. Tamborini, J.C. Tercero, J. Jimeno, M. D'Incalci, A. Gronchi, J.A. Fletcher, S. Pilotti, P.G. Casali, Efficacy of trabectedin (ecteinascidin-743) in advanced pretreated myxoid liposarcomas: a retrospective study, Lancet Oncol. 8 (7) (2007) 595–602, https://doi.org/10.1016/S1470-2045(07)70175-4.
[38] A.K. Larsen, C.M. Galmarini, M. D'Incalci, Unique features of trabectedin mechanism of action, Cancer Chemother. Pharmacol. 77 (4) (2016) 663–671, https://doi.org/10.1007/s00280-015-2918-1.
[39] D. Khemili, C. Valenzuela, F. Laraba-Djebari, D. Hammoudi-Triki, Differential effect of Androctonus australis hector venom components on macrophage KV channels: electrophysiological characterization, Eur. Biophys. J. 48 (1) (2019) 1–13, https://doi.org/10.1007/s00249-018-1323-1.
[40] M.A. Olivencia, M. Martinez-Casales, D.A. Peraza, A.B. Garcia-Redondo, G. Mondejar-Parreno, R. Hernanz, M. Salaices, A. Cogolludo, M.W. Pennington, C. Valenzuela, A.M. Briones, KV 1.3 channels are novel determinants of

macrophage-dependent endothelial dysfunction in angiotensin II-induced hypertension in mice, Br. J. Pharmacol. 178 (8) (2021) 1836–1854, https://doi.org/10.1111/bph.15407.
[41] A. Povo-Retana, M. Mojena, A.B. Stremtan, V.B. Fernandez-Garcia, A. Gomez-Saez, C. Nuevo-Tapioles, J.M. Molina-Guijarro, J. Avendano-Ortiz, J.M. Cuezva, E. Lopez-Collazo, J.F. Martinez-Leal, L. Bosca, Specific effects of trabectedin and lurbinectedin on human macrophage function and fate-novel insights, Cancers 12 (10) (2020), https://doi.org/10.3390/cancers12103060.
[42] T. Rao, Z. Tan, J. Peng, Y. Guo, Y. Chen, H. Zhou, D. Ouyang, The pharmacogenetics of natural products: a pharmacokinetic and pharmacodynamic perspective, Pharmacol. Res. 146 (2019), 104283, https://doi.org/10.1016/j.phrs.2019.104283.
[43] T. Roszer, Understanding the mysterious M2 macrophage through activation markers and effector mechanisms, Mediat. Inflamm. 2015 (2015), 816460, https://doi.org/10.1155/2015/816460.
[44] L. Virag, R.I. Jaen, Z. Regdon, L. Bosca, P. Prieto, Self-defense of macrophages against oxidative injury: Fighting for their own survival, Redox Biol. 26 (2019), 101261, https://doi.org/10.1016/j.redox.2019.101261.
[45] R. Vicente, N. Villalonga, M. Calvo, A. Escalada, C. Solsona, C. Soler, M. M. Tamkun, A. Felipe, Kv1.5 association modifies Kv1.3 traffic and membrane localization, J. Biol. Chem. 283 (13) (2008) 8756–8764, https://doi.org/10.1074/jbc.M708223200.
[46] N. Beyersdorf, A. Braun, T. Vogtle, D. Varga-Szabo, R.R. Galdos, S. Kissler, T. Kerkau, B. Nieswandt, STIM1-independent T cell development and effector function in vivo, J. Immunol. 182 (6) (2009) 3390–3397, https://doi.org/10.4049/jimmunol.0802888.
[47] Y. Gwack, S. Srikanth, M. Oh-Hora, P.G. Hogan, E.D. Lamperti, M. Yamashita, C. Gelinas, D.S. Neems, Y. Sasaki, S. Feske, M. Prakriya, K. Rajewsky, A. Rao, Hair loss and defective T- and B-cell function in mice lacking ORAI1, Mol. Cell Biol. 28 (17) (2008) 5209–5222, https://doi.org/10.1128/MCB.00360-08.
[48] C.A. McCarl, S. Khalil, J. Ma, M. Oh-hora, M. Yamashita, J. Roether, T. Kawasaki, A. Jairaman, Y. Sasaki, M. Prakriya, S. Feske, Store-operated Ca2+ entry through ORAI1 is critical for T cell-mediated autoimmunity and allograft rejection, J. Immunol. 185 (10) (2010) 5845–5858, https://doi.org/10.4049/jimmunol.1001796.
[49] M. Oh-Hora, M. Yamashita, P.G. Hogan, S. Sharma, E. Lamperti, W. Chung, M. Prakriya, S. Feske, A. Rao, Dual functions for the endoplasmic reticulum calcium sensors STIM1 and STIM2 in T cell activation and tolerance, Nat. Immunol. 9 (4) (2008) 432–443, https://doi.org/10.1038/ni1574.
[50] P.J. Hanley, M. Kronlage, C. Kirschning, A. Del Rey, F. Di Virgilio, J. Leipziger, I. P. Chessell, S. Sargin, M.A. Filippov, O. Lindemann, S. Mohr, V. Konigs, H. Schillers, M. Bahler, A. Schwab, Transient P2X7 receptor activation triggers macrophage death independent of Toll-like receptors 2 and 4, caspase-1, and pannexin-1 proteins, J. Biol. Chem. 287 (13) (2012) 10650–10663, https://doi.org/10.1074/jbc.M111.332676.
[51] C.M. Miller, N.R. Boulter, S.J. Fuller, A.M. Zakrzewski, M.P. Lees, B.M. Saunders, J. S. Wiley, N.C. Smith, The role of the P2X(7) receptor in infectious diseases, PLoS Pathog. 7 (11) (2011), e1002212, https://doi.org/10.1371/journal.ppat.1002212.
[52] F. Ginhoux, M. Guilliams, Tissue-resident macrophage ontogeny and homeostasis, Immunity 44 (3) (2016) 439–449, https://doi.org/10.1016/j.immuni.2016.02.024.
[53] G. Hoeffel, F. Ginhoux, Ontogeny of tissue-resident macrophages, Front. Immunol. 6 (2015) 486, https://doi.org/10.3389/fimmu.2015.00486.
[54] J. Sheng, C. Ruedl, K. Karjalainen, Most tissue-resident macrophages except microglia are derived from fetal hematopoietic stem cells, Immunity 43 (2) (2015) 382–393, https://doi.org/10.1016/j.immuni.2015.07.016.